ACS APPLIED MATERIALS & INTERFACES

Article

Thermally Triggered in Situ Assembly of Gold Nanoparticles for Cancer Multimodal Imaging and Photothermal Therapy

Mengmeng Sun, Dong Peng, Hanjun Hao, Jin Hu, Dongliang Wang, Kun Wang, Jing Liu, Ximin Guo, Yen Wei, and Weiping Gao

ACS Appl. Mater. Interfaces, **Just Accepted Manuscript** • DOI: 10.1021/acsami.6b16408 • Publication Date (Web): 08 Mar 2017

Just Accepted

ACS Publications

ACS Applied Materials & Interfaces is published by the American Chemical Society. 1155 Sixteenth Street N.W., Washington, DC 20036

Thermally Triggered *in Situ* Assembly of Gold Nanoparticles for Cancer Multimodal Imaging and Photothermal Therapy

Mengmeng Sun,[†] Dong Peng,[‡] Hanjun Hao,[†] Jin Hu,[†] Dongliang Wang,[§] Kun Wang,[‡] Jing Liu,[†] Ximin Guo,[$] Yen Wei,[⊥] and Weiping Gao[,†]*

[†]Department of Biomedical Engineering, School of Medicine, Tsinghua University, Beijing 100084, China

[‡] Key Laboratory of Molecular Imaging, Institute of Automation, Chinese Academy of Sciences, Beijing, 100190, China.

[§] CAS Key Laboratory for Biomedical Effects of Nanomaterials and Nanosafety, National Center for Nanoscience and Technology of China, Beijing 100190, China

[$] Department of Advanced Interdisciplinary Studies, Beijing Institute of Basic Medical Sciences, Beijing, 100850, China.

[⊥] Department of Chemistry, Tsinghua University, Beijing, 100084, China

*Corresponding author, E-mail: gaoweiping@tsinghua.edu.cn

ABSTRACT

The assembly of gold nanoparticles (AuNPs) to AuNP assemblies is of interest for cancer therapy and imaging. Herein we introduce a new and general paradigm, thermally triggered AuNP assembly, for the development of novel intelligent platforms for cancer photothermal therapy (PTT) and multimodal imaging. Site-specific conjugation of a thermally sensitive elastin-like polypeptide (ELP) to AuNPs yields thermally sensitive ELP-AuNPs. Interestingly, ELP-AuNPs can *in situ* form AuNP assemblies composed of short necklace-like gold nanostructures at elevated temperatures and thus show strong near-infrared light absorption and high photothermal effect. These thermally responsive properties of ELP-AuNPs enable simultaneous photothermal /photoacoustic /X-ray computed tomographic imaging and PTT of melanoma after single intratumoral injection of ELP-AuNPs. The thermally triggered assembly of a variety of nanoparticles with optical, electronic and magnetic properties into nanoparticle assemblies may open new ways for the establishment of intelligent platforms for various applications in biomedicine.

KEYWORDS: gold nanoparticle, elastin-like polypeptide, photothermal therapy, cancer therapy, hyperthermia

1. INTRODUCTION

Plasmonic nanostructures, particularly gold-based nanostructures such as gold nanorods and nanostars, are interesting in cancer photothermal therapy (PTT) and imaging.[1-8] Gold nanoparticles (AuNPs) typically possess localized surface plasmon resonance (LSPR) peaks in the visible region, which is not optimal for PTT and photoacoustic imaging (PAI) due to the low tissue penetration of visible light.[9] Near-infrared (NIR) light is preferred for PTT and PAI owing to its ability to penetrate soft tissues deeply.[10] Gold nanorods and nanostars represent a class of NIR photothermal transducers, which have been used for cancer photothermal therapy (PTT) and imaging.[3,11] However, these nanostructures are relatively hard to synthesize and scale up, and may suffer from chemical contamination from toxic surfactants. Alternatively, the assembly of AuNPs to AuNP assemblies allows the LSPR peaks to shift to the NIR region due to the plasmonic coupling effect between adjacent AuNPs, so that AuNP assemblies are capable of absorbing NIR light and then converting it into heat.[12-16] Furthermore, AuNPs are expected to be cleared from the body due to their small sizes after the dissociation of assemblies.[17,18] Typically, these AuNP assemblies are assembled from amphipathic polymer coated AuNPs[13-18] or are supramolecularly assembled from AuNPs and polymers through multivalent molecular recognition[14]. However, they depend on multi-step chemical synthesis of these functional polymers. Particularly, these synthetic polymers are not well-defined structurally and hard to be degraded to non-toxic species for the clearance from the body. Additionally, the large sizes of these AuNP assemblies, typically several hundred nanometers, may lead to the precipitation of them from the solutions to form larger aggregates during storage. Furthermore, large AuNP aggregates might be unfavorable for their diffusion from a single injection site into the whole tumor region for homogenous imaging and therapy.

Alternatively, pH-responsive small molecules are utilized to modify AuNPs to form pH-responsive AuNPs for cancer PTT.[19-21] These intelligent AuNPs well address the problems faced by the above AuNP assemblies, but the *in vivo* PTT efficacy is limited by the enhanced permeation and retention (EPR) effect, tumor acidity and tumor penetration that are highly dependent on the type, size, location and staging of tumors.[22-24] Most recently, we have demonstrated another intelligent theranostic platform based on salt-induced aggregation of AuNPs.[25] AuNPs without any surface modification can intratumorally aggregate into AuNP assemblies for cancer PAI and PTT. However, the salt-induced aggregation of AuNPs is susceptible to the local environments such as salt and protein concentrations, so that multiple injections are needed to achieve effective tumor imaging and therapy. Therefore, novel AuNP assembly strategies that can circumvent these limitations of the current methods are of interest for cancer therapy and imaging.

Herein, we report a new and general paradigm, thermally triggered assembly of AuNPs, to develop novel intelligent theranostic agents for cancer PTT and multimodal imaging. In this proof-of-concept study, a thermally sensitive elastin-like polypeptide (ELP) is site-specifically conjugated to AuNPs to form thermo-responsive ELP-AuNP conjugates (ELP-AuNPs) (Figure 1). ELP-AuNPs are soluble at room temperature but phase separate from the solution to form hierarchical AuNP assemblies upon single intratumoral injection (Figure 1). The AuNP assemblies are able to absorb NIR light and then convert it into heat due to the plasmonic coupling effect between adjacent AuNPs, enabling simultaneous multimodal imaging and PTT of melanoma.

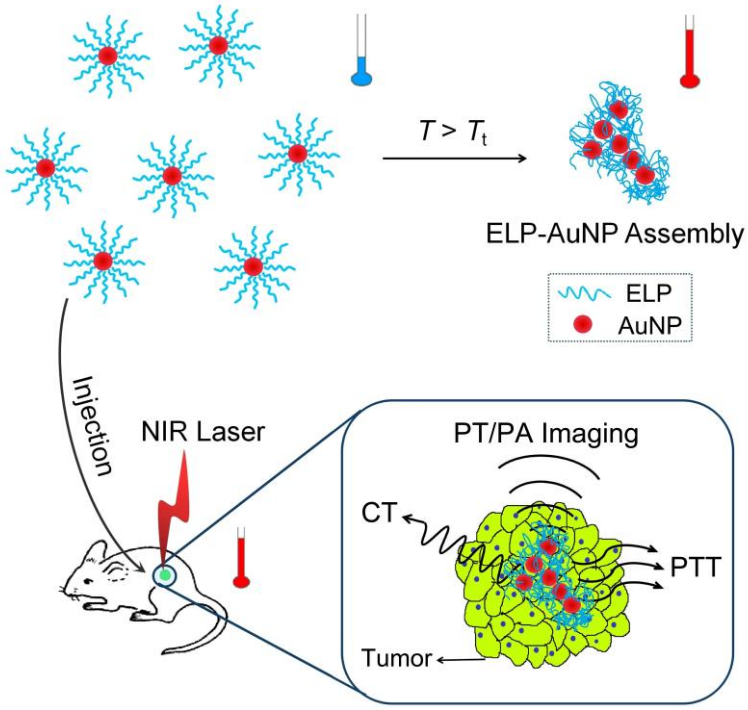

Figure 1. Scheme of the thermally triggered *in vitro* and *in vivo* assembly of ELP-AuNPs for X-ray computed tomographic (CT), photothermal (PT) and photoacoustic (PA) imaging and photothermal therapy (PTT) of tumor.

We chose ELPs as the thermo-responsive polymers for multiple reasons. First, ELPs are a class of biological polymers that consist of a repeat unit of Val-Pro-Gly-Xaa-Gly derived from human tropoelastin, in which the guest residue Xaa may be any amino acids except proline.[26] ELPs possess a specific phase transition temperature (T_t), above which they are insoluble and phase separate from aqueous solutions.[27] This phase transition behavior has been used to design injectable depots of drugs including radionuclide and peptide by attaching these drugs to ELPs.[28,29] Inspired by these applications in drug delivery, in this study, we, for the first time, hypothesized that conjugating ELPs to AuNPs would impart thermal sensitivity to the AuNPs to form injectable depots of AuNPs for multimodal imaging and PTT of cancer. Second, ELPs are non-toxic[30] and non-immunogenic[31], and can be biologically degraded into essential amino acid nutrients for the body[32,33]. Third, ELPs can be genetically engineered, so that their structure (e.g.

composition, molecular weight and polydispersity) and properties (e.g. T_t) can be controlled precisely. Fourth, ELPs are producible in *Escherichia coli* (*E. coli*) with high yield, which can be further purified by inverse transition cycling (ITC) that makes use of their phase transition behavior.[34,35] These unique attributes make ELPs more interesting than synthetic thermo-responsive polymers (e.g. poly(N-isopropylacrylamide)[36,37] and poly[di(ethylene glycol) methyl ether methacrylate])[38] that are non-biodegradable and toxic, especially in the design of thermally responsive polymer-AuNP conjugates that can form biodegradable, biocompatible and injectable AuNP assemblies for cancer therapy and imaging.

2. MATERIALS AND METHODS

2.1 Materials. $HAuCl_4 \cdot 3H_2O$, thiolated polyethylene glycol 1000 Da (HS-PEG) and other chemical reagents were provided by Sigma Aldrich. Restriction enzymes used for gene construction were New England Biolabs' products. All reagents for cell culture were from Gibco unless otherwise specified. The metastatic human C8161 melanoma cell line, expressing green fluorescent protein (GFP), was kindly donated by X. Guo (Beijing Institute of Basic Medical Sciences).

2.2 Preparation of ELP. The ELP (VGVPG) gene sequence, with cysteine at the N-terminus, in recombinant vector was constructed by recursive directional ligation by plasmid reconstruction (PRe-RDL) method.[39] *Escherichia coli* BL21 (DE3) (Invitrogen) was selected for ELP expression. The bacteria were cultured in Terrific Broth (TB) medium containing 100 mg/L kanamycin at 37 ℃ until OD_{600} was 0.6, and then induced to overexpress ELP by the addition of IPTG to 0.35 mM at 25 ℃ for 14 h. After centrifugation at 3000 rpm for 15 min, cell pellets were collected and dispersed in PBS (10 mM, pH 7.4), followed by ultrasonic breakage. After centrifugation, nucleic acids in the supernatant were removed by mixing with polyethyleneimine

(1% w/v). ELPs in the supernatant were further purified by ITC method.[40] The ITC was carried out by adding NaCl to 5 M at 40 ℃ to precipitate ELP out. After centrifugation of 12500 rpm at 40 ℃ for 15 min, the pellet with ELP was re-suspended in cold deionized water, followed by centrifugation at 4 ℃ to remove any insoluble components. 150 mg purified ELP was usually obtained from 1 L bacterial liquid. The concentration of ELP was determined by UV-visible spectrometry (Thermo Scientific) at 280 nm. The purity of ELP was further analyzed by sodium dodecyl sulfate polyacrylamide gel electrophoresis (SDS-PAGE).

2.3 Preparation of ELP-AuNPs. For synthesis of AuNPs, 45 mg $HAuCl_4 \cdot 3H_2O$ in 250 mL ultrapure water was brought to boil, to which 1 mL of trisodium citrate dihydrate (15% w/v) was rapidly added for another 5 min under vigorous stirring. After cooling down, an aqueous solution of ELP was added drop-wise to 10 μM, and the resulting mixture was sirred at 4 ℃ for 12 h. ELP-AuNPs were purified by centrifugation (14000 rpm for 1 h, 4 ℃) to get rid of residual ELP and re-dispersed in cold PBS. DLS (ZetaSizer, Malvern Instruments) was used to characterize ELP, AuNPs, and ELP-AuNPs at 20 ℃. The concentration of ELP on AuNPs was determined by a standard BCA assay, and the gold concentration was determined by ICP-MS. The yield of ELP-AuNPs with respect to the used quantity of ELP was 61%. Similarly, AuNPs were modified with HS-PEG to form PEG-AuNPs as a control.

2.4 Thermo-responsive Behavior of ELP-AuNPs. DLS (ZetaSizer, Malvern Instruments) was used to analyze the aggregation of the nanoparticles at different temperatures. Disposable cuvettes containing 200 μL samples at different concentrations were incubated from 15 ℃ to 30 ℃, and the hydrodynamic radius (R_h) of ELP-AuNPs was monitored every 2 ℃, or 0.2 ℃ (from 22 ℃ to 24 ℃) around the phase transition temperature (T_t). To determine the aggregation with time, ELP-AuNPs were incubated at 30 ℃ for different times, and mixed before analysis.

Then 200 μL samples were used for DLS assay at 30 ℃, and 2 mL ELP-AuNPs were used for the UV-Vis spectrometry assay at 30 ℃.

The size of ELP-AuNP assemblies from TEM images were all calculated by Image J software.

2.5 Photothermal Effect. 200 μL ELP-AuNPs solution at different gold concentrations in a disposable cuvette was incubated at 30 ℃ for 10 min and then exposed to the irradiation of an 808 nm laser at 0.5 , 1.0 , 1.5 or 2.5 W. The sample temperatures were recorded by using an infrared thermographic camera every 10 s. To calculate the photothermal conversion efficiency (η) of ELP-AuNPs, 1 mL of ELP-AuNPs (180 mg Au/L) in PBS was incubated at 30 ℃ for 10 min and then exposed to laser irradiation (808 nm, 1.5 W). When the temperature reached the maximum, the laser was switched off. The parameter η was calculated on the basis of the energy balance of the system.[41]

2.6 Cell Viability Assay. For MTT assay, the C8161 melanoma cells in DMEM/F-12 medium were placed in the 96-well plate with 4000 cells per well and cultured for 24 h at 37 ℃ and 5% CO_2, then 40 μL ELP-AuNPs samples with serial gold concentrations (0, 30, 60, 90, 105 and 120 mg/L) were added. After incubation for another 3 h, cells were under laser irradiation of 808 nm (2.5 W) for 3 min with spot diameter of 18 mm, followed by culture for another 1 h. The MTT reagents were added according to the instruction, followed by an incubation of 4 h. The absorbance at 490 nm of the mixture was determined by UV-Vis spectrometry (SpectraMax® M3 Microplate Reader, Molecular Devices) .

For *in vitro* PTT study, approximately $1*10^5$ C8161 cells in a 35-mm diameter dish were cultured overnight and then incubated with ELP-AuNPs (180 mg Au/L) for 3 h, followed by exposure to laser irradiation (808 nm, 2.5 W, 3 min, spot diameter of 10 mm). Dead cells were

stained in red with propidium iodide (PI), which was imaged by laser scanning confocal microscopy (LSM780, Zeiss).

2.7 Biocompatibility Study of ELP-AuNPs. Biocompatibility of ELP-AuNPs to human microvascular endothelial cells (HMECs) and murine fibroblasts 3T3 cells were investigated by MTT assay. Cells were placed in a 96-well plate at the density of 5000 cells/well. After 24 h, medium containing ELP-AuNPs at the final gold concentrations of 0, 30, 60, 90, 105, 120, 180 and 300 mg/L were added into the wells, followed by an incubation of 48 h. MTT assay was used to determine cell viability as described above.

2.8 Animal Models. Female BALB/c nude mice of 6 weeks (Vital River Laboratories, Beijing) were subcutaneously inoculated with a suspension of C8161 tumor cells ($2*10^6$) in DMEM/F-12 medium at the back. The tumor size was 150 mm^3 for *in vivo* imaging and 100-120 mm^3 for *in vivo* PTT.

2.9 *In Vivo* PT, PA and CT Imaging. For PT imaging, the tumors on mice were exposed to NIR irradiation (808 nm, 1.5 W, spot diameter of 8 mm), and the tumor temperature was recorded by using a GF300 infrared camera. These mice were under anesthesia during the experiments, which was enabled by intraperitoneal injection of 0.4 % pentobarbital sodium at the dose of 200 μL/20 g body weight.

PA imaging was performed by using a *MSOT inVision 512-echo* system (iTheraMedical, German) equipped with a 5 MHz,128-element linear array transducer on tumors. The mice were anesthetized by continuous isoflurane.

For CT imaging, ELP-AuNPs (100 μL, 600 mg Au/L) were intratumorally injected. CT scans and image analysis were conducted using SPECT/CT scanning system (Triumph X-SPECT/X-O CT, GMI Company, USA) at 45 min post-injection.

2.10 Photothermal Therapy. When the tumor volume reached 100-120 mm^3, C8161 tumor-bearing mice were divided to 6 groups (n=3-7 per group). For the ELP-AuNPs treated group, 100 μL of ELP-AuNPs (180 mg Au/L) was intratumorally injected with an incubation time of 45 min, followed by laser irradiation (808 nm, 1.5 W) for 7 min (n=7). Other groups were mice treated with PEG-AuNPs (100 μL, 180 mg Au/L) and irradiation (1.5 W, 7 min) (n=5), PBS (100 μL) and irradiation (1.5 W, 7 min) (n=5), ELP-AuNPs (100 μL, 180 mg Au/L) (n=3), PEG-AuNPs (100 μL, 180 mg Au/L) (n=3), and PBS (100 μL) (n=3). The laser spot diameter used for therapy is 8 mm to cover entire tumors. The body weights and tumor volumes of mice were measured every three days post treatment. Tumor volume (*V*) was determined by the following equation: $V=AB^2/2$, in which *A* and *B* are the length and width of tumors, respectively. The mice with tumor volumes over 1200 mm^3 or weight loss over 15% were executed.

2.11 Biodistribution Study. For biodistribution study, 18 μg ELP-AuNPs was intratumorally injected to C8161 tumor-bearing mice. After an incubation of 45 min, the tumors were exposed to laser irradiation (808 nm, 1.5 W, 7 min). Then, the mice were killed immediately (n=3) or a month later (n=3) to collect all organs and tumors or scars. These samples were dried and digested by heating in the 3:1 HCl/HNO_3 mixture. For quantification, the gold concentrations of organs were determined by inductively coupled plasma mass spectrometry (ICP-MS) (ELAN DRC-e, Perkin Elmer, USA) and converted to the percentage of the injection dose.

2.12 H&E Staining/ TEM/ Freezing Slice of Tumors. The mice with C8161 tumors (80-100 mm^3) on back were intratumorally injected with ELP-AuNPs (100 μL, 180 mg Au/L), followed by an incubation of 45 min. After exposure to laser irradiation (808 nm, 1.5 W) for 7 min, the tumors were collected.

For TEM assay, the obtained tumors were fixed in normal saline with 2.5 % glutaraldehyde before cut into pellets. Pellets were fixed again, dehydrated, embedded in Epon, and cut into slices (70 nm in thickness). The slices were analyzed by TEM and EDS (Hitichi-H-7650B, Japan). For H&E staining, the tumor was fixed in a formaldehyde solution, then dehydrated, sliced to a thickness of 5.0 μm, followed by H&E staining assay. For fluorescence imaging, the tumor was embedded, frozen and fixed in optimal cutting temperature compound (OCT), then processed to 8 μm slides at -20 ℃. The tumor slides were observed by an Invert fluorescence microscope (Eclipse 90i, Nikon, Japan).

2.13 Statistical Analysis. All data were showed as mean ± standard deviation. In MTT assay and *in vivo* biodistribution assay, each group had three separate experiments. For *in vivo* PTT, the animal quantity of each treatment group was described as above. The differences between two groups were analyzed by a two-tailed, unpaired Student's t-test. One (*), two (**) and three stars (***) mean statistical significance at $P < 0.05$, 0.01 and 0.001, respectively.

3. RESULTS AND DISCUSSION

3.1 Synthesis and Characterization of ELP-AuNPs. To ensure that ELP-AuNPs are injectable at room temperature but can phase separate from the solution to form AuNP assemblies upon intratumoral injection, an ELP was engineered genetically to have 60 pentameric repeats in which the Xaa = Val (Figure S1), which had concentration-dependent T_t's that were above room temperature but below body temperature (Figure S2). Cysteine was fused at the N-terminal end of ELP for N-terminal conjugation of the ELP to AuNPs through the covalent bonding of gold-thiol. The formed ELP-AuNPs had a hydrodynamic radius (R_h) of 23.4 nm, which was bigger than those of the pristine AuNPs (9.7 nm) and the ELP (4.8 nm) (Figure

2a). The LSPR peak of AuNPs slightly shifted from 520 nm to 525 nm after the ELP conjugation (Figure S3a), as expected. Upon heating, ELP-AuNPs showed sharp phase transition behaviors with T_t values above 21 ℃ that were dependent on gold concentration (Figure 2b,c). The thermal responsibility of ELP-AuNPs at the gold concentration of 120 mg/L was confirmed by transmission electron microscopy (TEM) (Figure 2d). At 20 ℃, ELP-AuNPs were monodisperse with an average diameter of 15 nm. As the temperature rose up to 22 ℃ and 23 ℃, small loose AuNP assemblies and large tight AuNP assemblies were observed, respectively. Up to 30 ℃, larger and tighter AuNP assemblies were observed, which had an average diameter of 870 nm. Intriguingly, these AuNP assemblies were mainly composed of a number of short necklace-like gold nanostructures with different lengths (Figure 2d, inset), which could not be observed for both pH-induced assembly of AuNPs[19-21] and salt-induced assembly of AuNPs[25]. Together, these data indicated that the size of AuNP assemblies was temperature dependent. Additionally, at 30 ℃, the size of AuNP assemblies increased with the gold concentration (Figure S4).

The assembly kinetics of ELP-AuNPs at the gold concentration of 120 mg/L at 30 ℃ was further studied by dynamic light scattering (DLS), TEM and UV-Vis-NIR absorption spectrometry. The R_h of ELP-AuNPs rapidly increased from 30 to 940 nm when the time increased from 0 to 20 min, and then remained almost constant (Figure 2e). It should be noted that an apparent precipitation of AuNP assemblies was observed after 20 min incubation due to their large size. This was confirmed by TEM, which showed that AuNP assemblies became larger and more compact with the time (Figure S5). Interestingly, the LSPR peak of ELP-AuNPs gradually shifted and broadened, and the absorption in the NIR region gradually increased when the time increased from 0 to 45 min (Figure 2f), due to the interparticle plasmonic coupling effect[42]. Additionally, ELP-AuNPs were pH-irresponsible, as indicated by the pH-independent

R_h, LSPR peak and T_t of ELP-AuNPs (Figure S6). In a control experiment, AuNPs were modified with a thermally irresponsive polymer, poly(ethylene glycol) (PEG) to form PEG-AuNPs as a thermally irresponsive control (Figure S3b), as indicated by the temperature-independent R_h and LSPR peak of PEG-AuNPs (Figure S7). These results indicate that ELP-AuNPs are thermo-responsive plasmonic nanostructures.

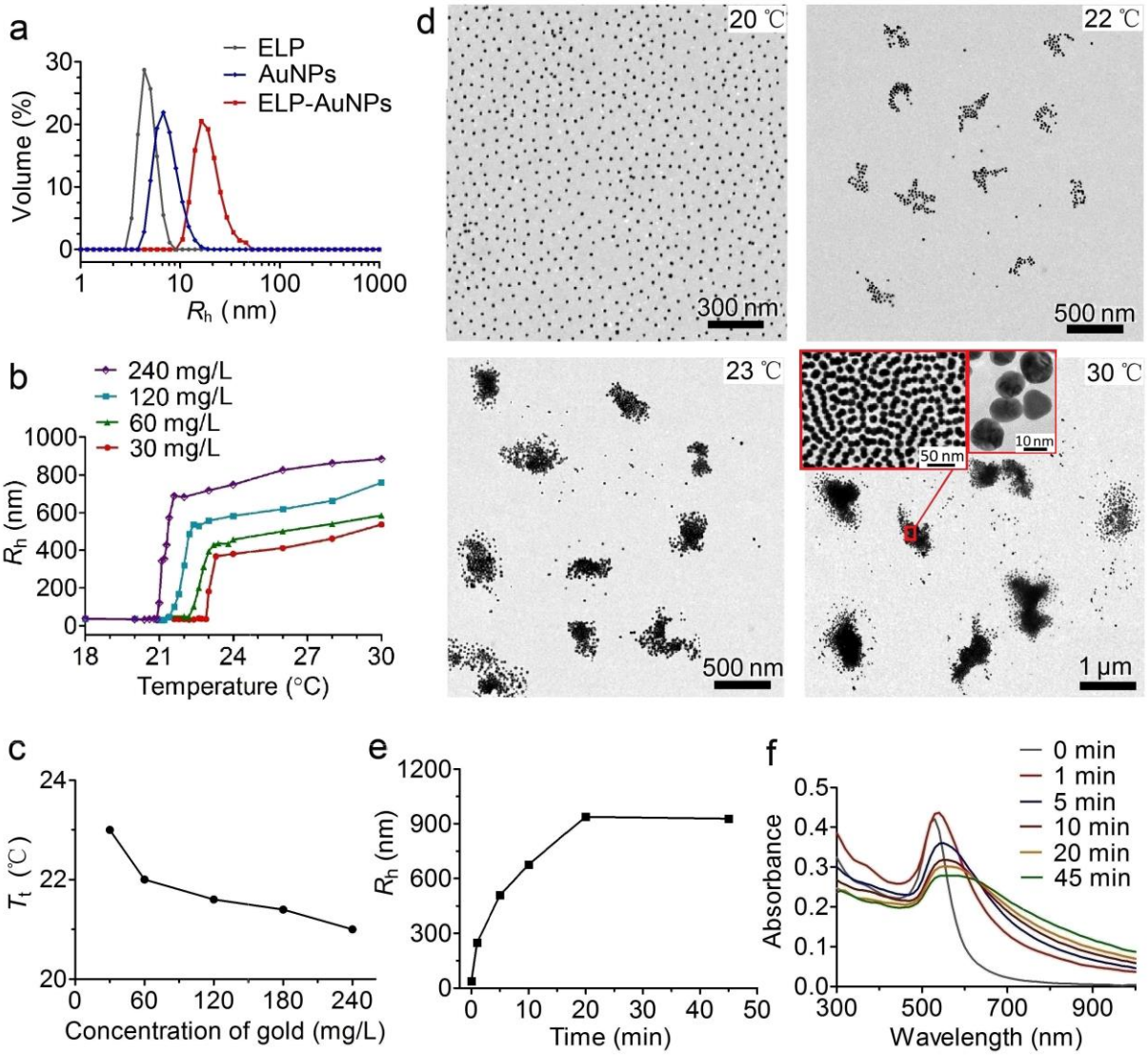

Figure 2. Physicochemical characterization of ELP-AuNPs. (a) DLS profiles of ELP, AuNPs and ELP-AuNPs. R_h denotes hydrodynamic radius. (b) The hydrodynamic radius (R_h) of ELP-AuNPs at different gold concentrations as a function of temperature. (c) The gold concentration

dependence of the phase transition temperature (T_t) of ELP-AuNPs in PBS. (d) The TEM images of ELP-AuNPs at the gold concentration of 120 mg/L in PBS after incubation for 10 min at 20 ℃, 22 ℃, 23 ℃ and 30 ℃. (e) The time dependence of R_h of ELP-AuNPs (120 mg Au/L) at 30 ℃. (f) The absorption spectra of ELP-AuNPs at the gold concentration of 120 mg/L in PBS after incubation for different times at 30 ℃.

3.2 Photothermal Effect of ELP-AuNPs. Inspired by the intriguing thermo-responsive findings, we hypothesized that thermally responsive ELP-AuNPs would be thermally responsive NIR photothermal transducers. At first, we studied the photothermal effect of ELP-AuNPs at 30 ℃ at different gold concentrations (Figure 3a). Upon 808 nm laser irradiation, the solution temperature of ELP-AuNPs in PBS quickly increased to high temperatures, which depended on the gold concentration. For instance, the solution temperature was raised by 60 ℃ when the gold concentration was 300 mg/L. In contrast, PEG-AuNPs did not show obvious photothermal effect (Figure S8), as expected. Additionally, ELP-AuNPs showed an increase in photothermal effect as the laser power density increased (Figure 3b). Interestingly, at a laser irradiation-induced temperature of 70 ℃ or after laser irradiation, large and compact AuNP assemblies mainly composed of necklace-like gold nanostructures were observed (Figure 3c,d). The photothermal conversion efficiency (η) of ELP-AuNPs was calculated to be ca. 30%, which was higher than that of PEG-AuNPs (21%) (Figure S9). All of the results suggest that thermally responsive ELP-AuNPs are highly efficient photothermal transducers.

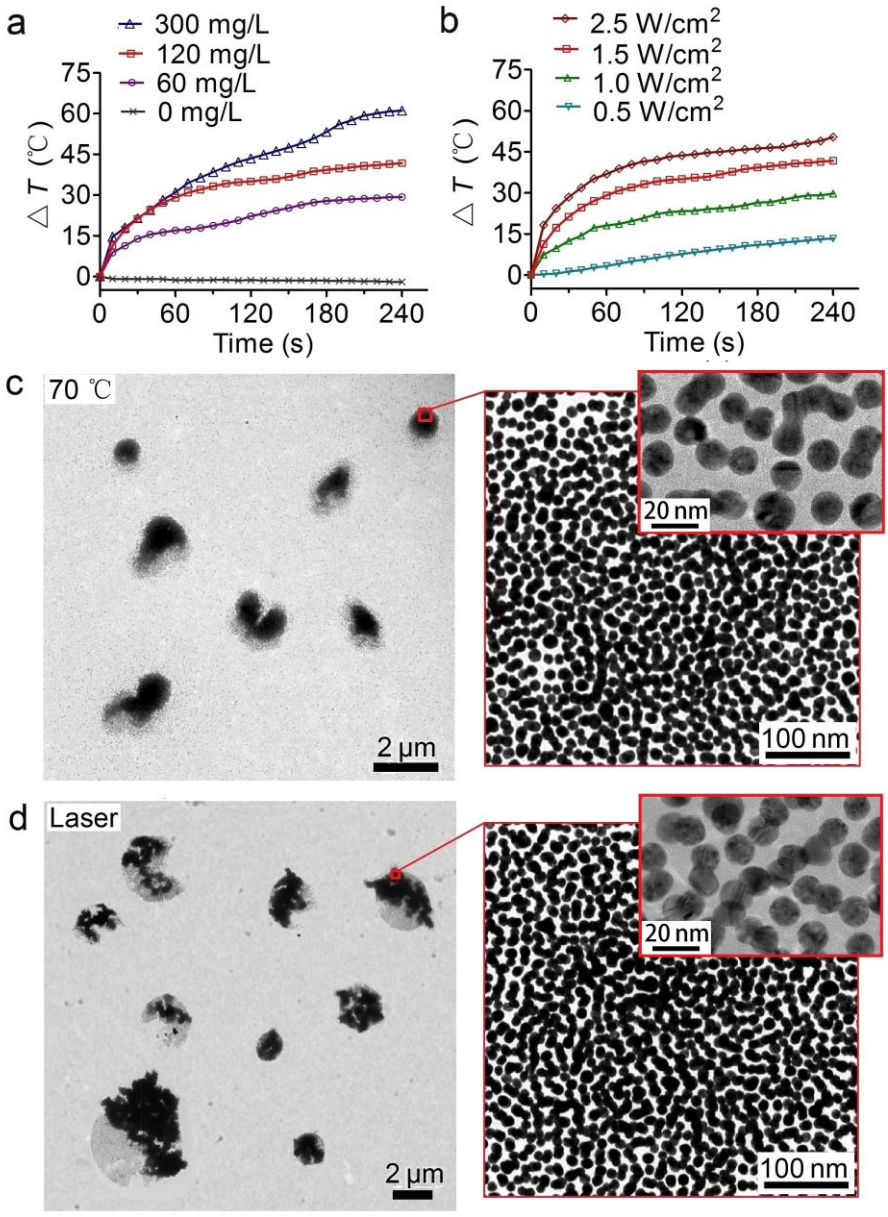

Figure 3. Photothermal effect of ELP-AuNPs. (a) The gold concentration dependence of temperature of the PBS solution of ELP-AuNPs exposed to laser irradiation (808 nm, 1.5 W, 4 min), after incubation for 10 min at 30 ℃. (b) The heating curves of ELP-AuNPs (120 mg Au/L) in PBS at different laser power densities, after incubation for 10 min at 30 ℃. Δ*T* denotes the temperature evolution. (c) The TEM images of ELP-AuNPs (120 mg Au/L) in PBS after incubation for 10 min at 70 ℃. (d) The TEM images of ELP-AuNPs (120 Au mg/L) after incubation for 10 min at 30 ℃ and then laser irradiation.

3.3 *In Vitro* Photothermal Cytotoxicity of ELP-AuNPs. Next, we studied the photothermal cytotoxicity of ELP-AuNPs against cancer cells at 37 ℃ (Figure 4). ELP-AuNPs did not show

toxicity to C8161 melanoma cancer cells (Figure 4a(i)) and normal cells such as murine fibroblast 3T3 cells and human microvascular endothelial cells (Figure S10), suggesting that ELP-AuNPs themselves are biocompatible. Upon laser irradiation (808 nm, 2.5 W, 3 min), they showed cytotoxicity at the gold concentration of 60 mg/L, and caused all of cancer cells to death when the gold concentration reached 180 mg/L (Figure 4a(i)). In contrast, PEG-AuNPs did not show any cytotoxicity to cancer cells upon laser irradiation (Figure 4a(ii)).

Cancer cells were also stained with propidium iodide (PI) to identify dead cells (red) from live ones (green) (Figure 4b). Cancer cells treated with ELP-AuNPs or laser irradiation showed green fluorescence, indicating that cancer cells did not die after the treatment with either laser irradiation (Figure 4b(ii)) or ELP-AuNPs (Figure 4b(iii)). In contrast, all of cancer cells in the laser spot looked dead after they were treated with ELP-AuNPs plus laser irradiation, as indicated by the red fluorescence (Figure 4b(iv)). In contrast, cancer cells outside the irradiated region displayed green fluorescence, indicating the high selectivity and localization of PTT with ELP-AuNPs. As expected, PEG-AuNPs or PEG-AuNPs plus laser irradiation did not cause any cell death, as demonstrated by the green fluorescence (Figure 4b(v),(vi)). Taken together, the results reveal that ELP-AuNPs are highly efficient for PTT of cancer cells.

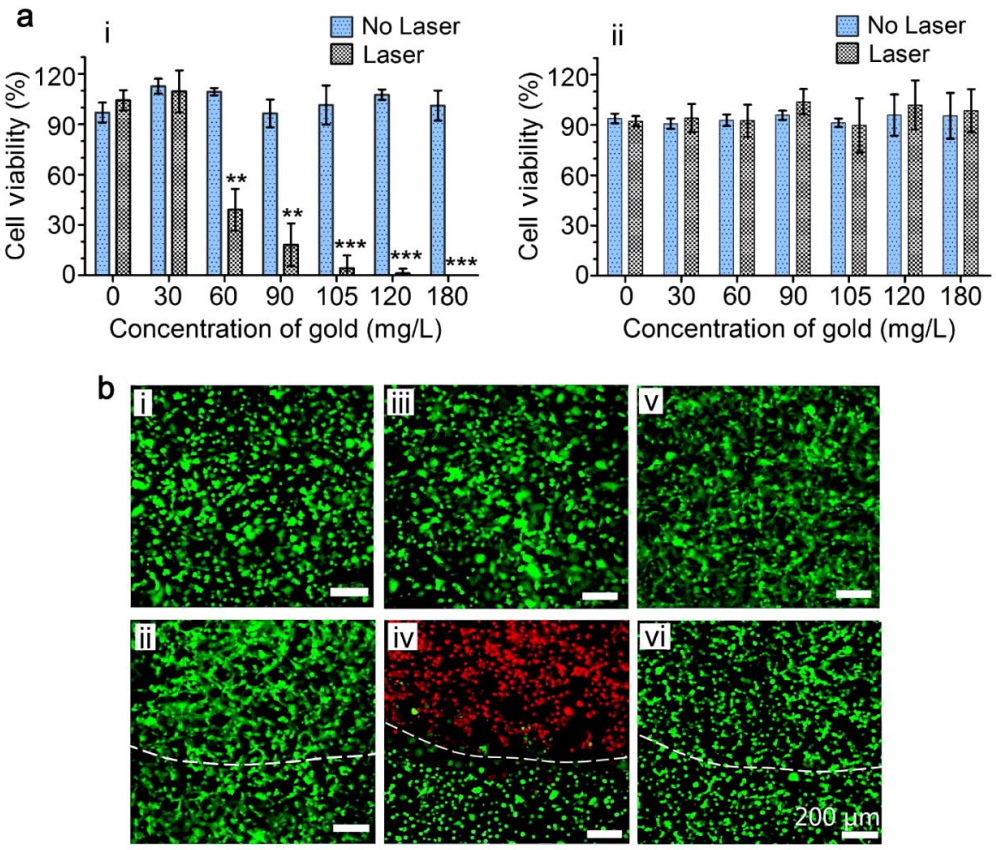

Figure 4. Photothermal cytotoxicity of ELP-AuNPs against C8161 melanoma cancer cells. (a) Cell viability of C8161 cells after treatment with ELP-AuNPs (i) and PEG-AuNPs (ii). Laser irradiation: 808 nm, 2.5 W, 3 min, spot diameter of 18 mm. (b) Fluorescence images of C8161 melanoma cells expressing green fluorescent protein (green) after different treatments: no treatment (i), laser irradiation (ii), ELP-AuNPs (180 mg Au/L) (iii), ELP-AuNPs (180 mg Au/L) plus laser irradiation (iv), PEG-AuNPs (180 mg Au/L) (v), and PEG-AuNPs (180 mg Au/L) plus laser irradiation (vi). Laser irradiation: 808 nm, 2.5 W, 3 min, spot diameter of 10 mm.

3.4 *In Vivo* Multimodal Imaging. We further hypothesized that ELP-AuNPs would be injectable into tumors to *in situ* form AuNP assemblies for *in vivo* PTI, PAI, CTI and PTT as the intratumoral temperature (ca. 32 ℃) is well above the T_t (ca. 23 ℃) of ELP-AuNPs. First, we investigated the intratumoral assembly of ELP-AuNPs in a C8161 melanoma xenograft model by TEM (Figure 5a) and energy dispersive X-ray spectroscopy (EDS) (Figure S11). Upon single intratumoral injection, ELP-AuNPs formed AuNP assemblies, whereas PEG-AuNPs were well dispersed in the tissue. It should be pointed out that ELP-AuNPs and PEG-AuNPs could be

rinsed away from the tissue slices during the TEM sample preparation processes, so that it was nontrivial to do such a kind of TEM imaging.

Second, we monitored the local tumor temperature change by thermal imaging (Figure 5b, c). Interestingly, the local tumor temperature of mice treated with ELP-AuNPs was sharply increased by nearly 28 ℃ within 10 seconds and reached a very high temperature of 65.9 ℃ within 7 min, which are highly favorable to thermally destroy tumor cells *in vivo*. Meanwhile, the temperatures in other body parts of the mice did not increase significantly, showing that the photothermal effect was selective and localized at the tumor site. In contrast, the local tumor temperature of mice treated with PEG-AuNPs or PBS was just increased to 42.6 ℃ or 41.2 ℃, respectively, which is not so high for the destruction of tumor cells *in vivo*.

Third, we evaluated the *in vivo* PA property of ELP-AuNPs (Figure 5d). A PA signal was quickly detected upon intratumoral injection of ELP-AuNPs and became homogeneous and intense with the time, indicating that ELP-AuNPs could diffuse from the injection site into the whole tumor region. When the PA signal increased to the maximum at 45 min after injection, its intensity decreased with the time (Figure 5e), suggesting that some ELP-AuNPs might be cleared from the tumor site and enter the circulation system. In contrast, no significant PA signal was detected for the treatment with PEG-AuNPs. Fourth, we examined the *in vivo* CT property of ELP-AuNPs (Figure 5f). As expected, an obvious CT signal was observed after single intratumoral injection of ELP-AuNPs or PEG-AuNPs plus 45 min incubation.

Taken together, these results show that ELP-AuNPs are highly efficient multimodal imaging agents for PTI, PAI and CTI of cancer.

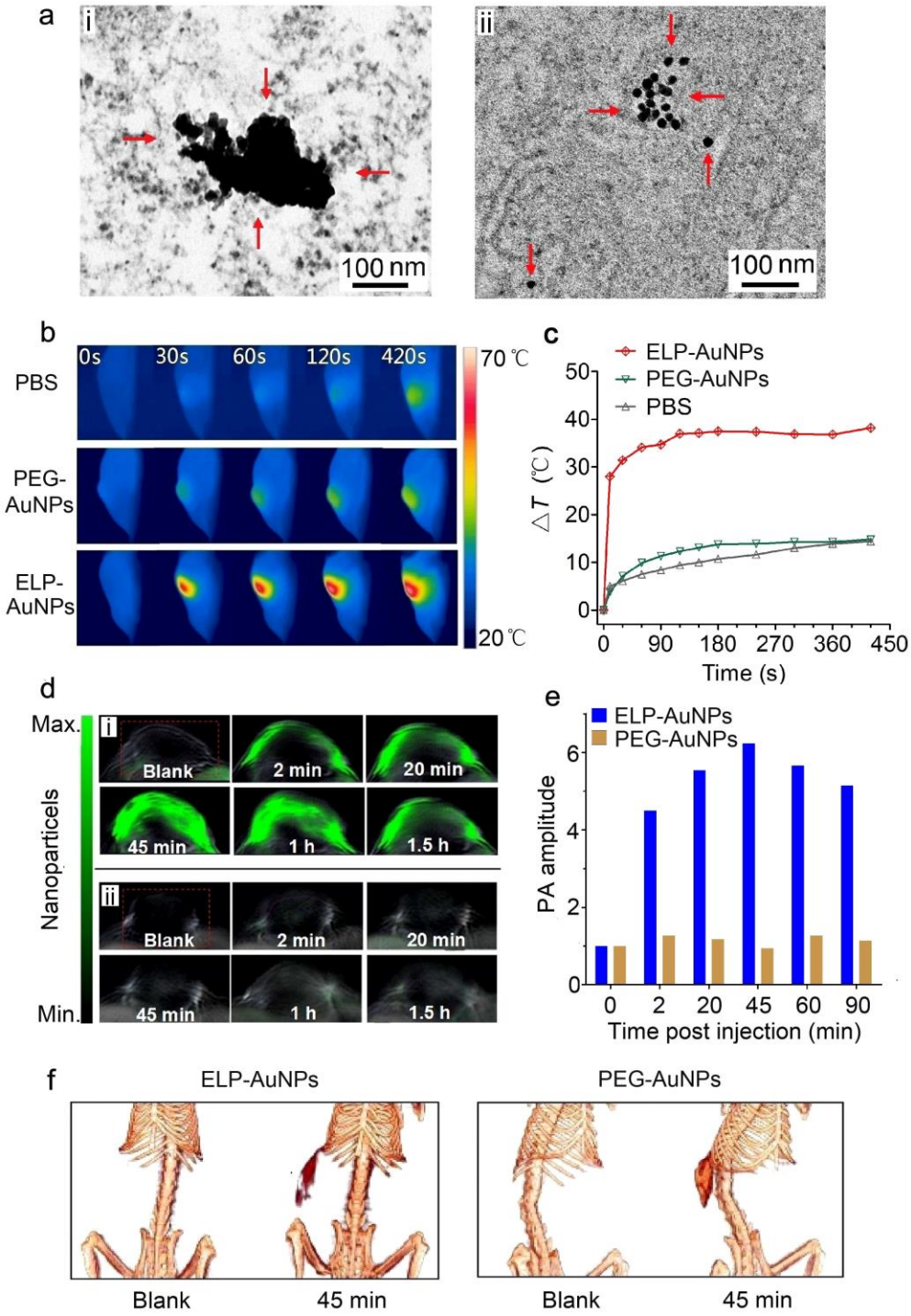

Figure 5. *In vivo* multimodal imaging of tumors post single intratumoral injection of ELP-AuNPs. (a) TEM images of tumor tissues containing ELP-AuNPs (i) and PEG-AuNPs (ii). (b) Infrared thermal images of mice bearing C8161 tumors treated with PBS, ELP-AuNPs (18 μg Au) and PEG-AuNPs (18 μg Au) under laser irradiation (1.5 W). (c) The temperature evolution (ΔT) of tumors treated with PBS, ELP-AuNPs (18 μg Au) and PEG-AuNPs (18 μg Au) upon laser irradiation. (d) PA images of tumor tissues before and after single injection of 18 μg ELP-AuNPs

(i) and 18 μg PEG-AuNPs (ii). (e) PA intensity of tumor tissue treated with ELP-AuNPs or PEG-AuNPs as a function of time. (f) Three-dimensional CT images of tumor tissue before and after single injection of ELP-AuNPs (60 μg) or PEG-AuNPs (60 μg).

3.5 *In Vivo* Photothermal therapy. We further studied *in vivo* PTT enabled by ELP-AuNPs. Guided by these multimodal images, PTT was conducted at 45 min post single injection of ELP-AuNPs (18 μg Au) (Figure 6). In the group administered with ELP-AuNPs plus laser irradiation (808 nm, 1.5 W, 7 min, laser beam diameter of 8 mm), the tumors were abolished, resulting in black scars at the tumor sites (Figure 6a and Figure S12). In contrast, no significant inhibition on tumor growth was found in other groups treated with ELP-AuNPs, PBS, PBS plus laser irradiation, PEG-AuNPs alone, and PEG-AuNPs plus laser irradiation. The outperformance of ELP-AuNPs over PEG-AuNPs in inhibition on tumor growth was correlated with a significant improvement in animal survival (Figure 6b). In contrast to the short average life spans of 6-18 days in other groups, no death and tumor recurrence were observed in the ELP-AuNPs plus laser irradiation treated group. There was no loss of body weight in all the groups post the treatments (Figure S13). Notably, the laser density here (1.5 W, laser spot diameter of 8 mm) was higher than the limit irradiation of skin (0.3 W/cm^2) according to the ANSI regulation[43], but there was no obvious damage for mice in control groups (Figure 6a, Figure S12 and S13). These results indicate that ELP-AuNPs are highly efficient for *in vivo* PTT of cancer.

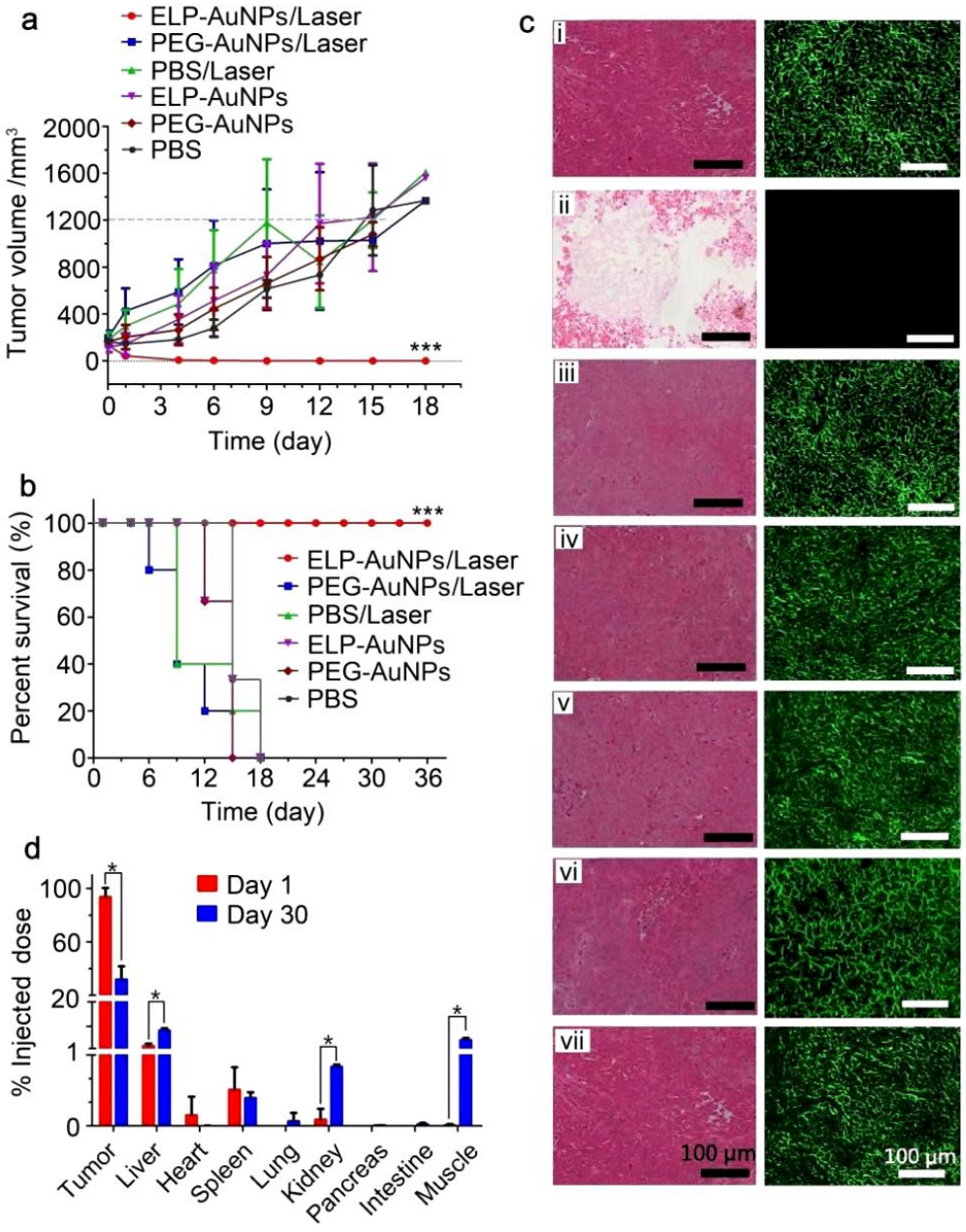

Figure 6. *In vivo* PTT after single intratumoral injection of ELP-AuNPs. (a) Tumor growth after different treatments in a C8161 tumor mouse model. Laser irradiation: 808 nm, 1.5 W, 7 min. (b) Survival curves of C8161 tumor-bearing mice post different treatments. (c) H&E staining (left) and fluorescent images (right) of tumor tissue slices of different groups of mice: no treatment (i), ELP-AuNPs plus laser (ii), PEG-AuNPs plus laser (iii), PBS plus laser (iv), ELP-AuNPs (v), PEG-AuNPs (vi) and PBS (vii). (d) Biodistribution of gold at 1 day and 30 days after single intratumoral injection of ELP-AuNPs followed by laser irradiation.

3.6 Histology Assay and Biodistribution. The superiority of ELP-AuNPs over PEG-AuNPs in PTT was further verified by hematoxylin and eosin (H&E) staining. Significant damage of cancer cells was observed in the tumors of the ELP-AuNPs plus laser irradiation treated group (Figure 6c(ii)), but not in the tumors of other groups. This result was confirmed by fluorescence imaging of tumor slices, as indicated by the presence of fluorescence in the control groups but the absence of fluorescence in the ELP-AuNPs plus laser irradiation treated group (Figure 6c).

We also investigated gold biodistribution after single intratumoral injection of ELP-AuNPs plus laser irradiation (Figure 6d). Almost all of gold stayed in the tumor tissue on day 1; however, on day 30, only 34% of gold remained in the tumor tissue and more gold was observed in liver, kidney, suggesting that the assemblies of ELP-AuNPs could disassemble into smaller particles to be cleared from the tumor site and enter the circulation system, and thus could be cleared from the body under the physiological conditions over time.[44,45] This might be ascribed to the biodegradability of ELP component that can be degraded by proteases into amino acids in vivo.[32,33] Notably, a more detailed biodistribution study will be carried out to make clear the mechanism of the clearance in the future. Collectively, all of the results demonstrate that ELP-AuNPs are highly efficient in multimodal imaging and PTT of cancer

4. CONCLUSIONS

In conclusion, we demonstrate that thermally responsive ELP-AuNPs constructed by site-specific conjugation of a thermally responsive ELP to AuNPs can phase separate from the solution to form AuNP assemblies composed of short necklace-like or worm-like gold nanostructures as the solution temperature is higher than the T_t of ELP-AuNPs. This thermally triggered AuNP assembly enabled by ELP-AuNPs leads to several findings that are important for

developing intelligent theranostic agents for cancer therapy and imaging. First, ELP-AuNPs can efficiently absorb NIR light and convert it into heat due to the plasmonic coupling effect between adjacent AuNPs of AuNP assemblies when the solution temperature is above their T_t, enabling *in vitro* photothermal cytotoxicity. Second, ELP-AuNPs are injectable into tumors to *in situ* form AuNP assemblies as novel intelligent theranostic agents, enabling *in vivo* multimodal imaging and PTT of cancer. Third, ELP-AuNPs are biocompatible and can be cleared from the body, which are favorable for the translation into the clinic. Fourth, ELP-AuNPs are as small as dozens of nanometers so that they are stable enough for long-time storage and can diffuse into the whole tumor tissue for homogeneous imaging and therapy. Fifth, ELP-AuNPs are not dependent on the tumor and intracellular microenvironments and EPR effect but on the tumor temperature, which may make them practical for the treatment of a variety of tumors. Sixth, PTT is applicable to superficial tumors such as melanoma, neck and bladder cancers, which justifies the usefulness of intratumoral injection of ELP-AuNPs. These unique attributes make ELP-AuNPs interesting as novel intelligent theranostic agents for cancer therapy and imaging. We believe that the thermally triggered assembly of AuNPs enabled by site-specific ELP conjugation is applicable to a variety of nanoparticles with optical, magnetic and electronic properties to form nanoparticle assemblies for biomedical applications. Based on these findings, it is promising to further develop thermally responsive nanoparticles for thermal targeting, imaging and therapy of cancer after intravenous injection.

ASSOCIATED CONTENT

Supporting Information

The Supporting Information is available free of charge on the ACS Publications website at DOI: 10.1021/acsami..

The purification and phase transition behavior of ELP, absorption curves of ELP-AuNPs at different temperatures or pH values, TEM analyses of ELP-AuNP assemblies, heating curves and photothermal efficiency of ELP-AuNP assemblies, biocompatibility of ELP-AuNPs, and digital pictures and the change of body weight of mice after treatments (PDF)

AUTHOR INFORMATION

Corresponding Author

*E-mail: gaoweiping@tsinghua.edu.cn

Present Address

[†]Department of Biomedical Engineering, School of Medicine, Tsinghua University, Beijing 100084, China

Notes

The authors declare no competing financial interest.

ACKNOWLEDGMENT

This study was financially supported by Beijing Natural Science Foundation（2172028）.

REFERENCES

(1) Hirsch, L.; Stafford, R. J.; Bankson, J. A.; Sershen, S. R.; Rivera, B.; Price, R. E.; Hazle, J. D.; Halas, N. J.; West, J. L. Nanoshell-mediated Near-infrared Thermal Therapy of Tumors under Magnetic Resonance Guidance. *Proc. Natl. Acad. Sci. U. S. A.* **2003**, *100,* 13549-13554.

(2) Huang, X.; El-Sayed, I. H.; Qian, W.; El-Sayed, M. A. Cancer Cell Imaging and Photothermal Therapy in the Near-infrared Region by Using Gold Nanorods. *J. Am. Chem. Soc*. **2006**, *128*, 2115-2120.

(3) Liu, X.; Huang, N.; Li, H.; Wang, H.; Jin, Q.; Ji, J. Multidentate Polyethylene glycol Modified Gold Nanorods for In Vivo Near-Infrared Photothermal Cancer Therapy. *ACS Appl. Mater. Interfaces* **2014**, *6*, 5657-5668.

(4) Sironi, L.; Freddi, S.; Caccia, M.; Pozzi, P.; Rossetti, L.; Pallavicini, P.; Donà, A.; Cabrini, E.; Gualtieri, M.; Rivolta, I.; Panariti, A.; D'Alfonso, L.; Collini, M.; Chirico, G. Gold Branched Nanoparticles for Cellular Treatments. *J Phys. Chem. C* **2012**, *116*, 18407-18418.

(5) Liu, Y.; Ashton, J. R.; Moding, E. J.; Yuan, H.; Register, J. K.; Fales, A. M.; Choi5, J.; Whitley, M. J.; Zhao, X.; Qi, Y.; Ma, Y.; Vaidyanathan, G.; Zalutsky, M. R.; Kirsch, D. G.; Badea, C. T.; Vo-Dinh, T. A Plasmonic Gold Nanostar Theranostic Probe for In Vivo Tumor Imaging and Photothermal Therapy. Theranostics **2015**, *5*, 946-960.

(6) Jain, P. K.; Huang, X.; El-Sayed, I. H.; El-Sayed, M.A. Noble Metals on the Nanoscale: Optical and Photothermal Properties and Some Applications in Imaging, Sensing, Biology, and Medicine. *Acc. Chem. Res*. **2008**, *41*, 1578-1586.

(7) Chen, J.; Glaus, C.; Laforest, R.; Zhang, Q.; Yang, M.; Gidding, M.; Welch, M. J.; Xia, Y. Gold Nanocages as Photothermal Transducers for Cancer Treatment. *Small* **2010**, *6*, 811-817.

(8) Ye, E.; Win, K. Y.; Tan, H. R.; Lin, M.; Teng, C. P.; Mlayah, A.; Han, M. Y. Plasmonic Gold Nanocrosses with Multidirectional Excitation and Strong Photothermal Effect. *J. Am. Chem. Soc.* **2011**, *133*, 8506-8509.

(9) Khlebtsov, N.; Bogatyrev, V.; Dykman, L.; Khlebtsov, B.; Staroverov, S.; Shirokov, A.; Matora, L.; Khanadeev, V.; Pylaev, T.; Tsyganova, N.; Terentyuk, G. Analytical and Theranostic Applications of Gold Nanoparticles and Multifunctional Nanocomposites. *Theranostics* **2013**, *3*, 167-180.

(10) Weissleder, R. A Clearer Vision for In Vivo Imaging. *Nat. Biotechnol*. **2001**, *19*, 316-316.

(11) Pallavicini, P.; Dona`, A.; Casu, A.; Chirico, G.; Collini, M.; Dacarro, G.; Falqui, A.; Milanese, C.; Sironic, L.; Tagliettia, A. Triton X-100 for Three-plasmon Gold Nanostars with Two Photothermally Active NIR (Near IR) and SWIR(Short-wavelength IR) Channels. *Chem. Commun*. **2013**, *49*, 6265-6267.

(12) Wang, S.; Chen, K.; Wu, T. H.; Wang, H.; Lin, W. Y.; Ohashi, M.; Chiou, P. Y.; Tseng, H. R. Photothermal Effects of Supramolecularly Assembled Gold Nanoparticles for the Targeted Treatment of Cancer Cells. *Angew. Chem., Int. Ed.* **2010**, *49*, 3777-3781.

(13) Lin, J.; Wang, S.; Huang, P.; Wang, Z.; Chen, S.; Niu, G.; Li, W.; He, J.; Cui, D.; Lu, G.; Chen, X.; Nie, Z. Photosensitizer-loaded Gold Vesicles with Strong Plasmonic Coupling Effect for Imaging-guided Photothermal/Photodynamic Therapy. *ACS Nano* **2013**, *7*, 5320-5329.

(14) He, J.; Huang, X.; Li, Y. C.; Liu, Y.; Babu, T.; Aronova, M. A.; Wang, S.; Lu, Z.; Chen, X.; Nie, Z. Self-assembly of Amphiphilic Plasmonic Micelle-like Nanoparticles in Selective Solvents. *J. Am. Chem. Soc*. **2013**, *135*, 7974-7984.

(15) Huang, P.; Lin, J.; Li, W.; Rong, P.; Wang, Z.; Wang, S.; Wang, X.; Sun, X.; Aronova, M.; Niu, G; Leapman, R. D.; Nie, Z.; Chen, X. Biodegradable Gold Nanovesicles with an Ultrastrong Plasmonic Coupling Effect for Photoacoustic Imaging and Photothermal Therapy. *Angew. Chem*. **2013**, *125*, 14208-14214.

(16) Huang, C. C.; Liu, T. M. Controlled Au-Polymer Nanostructures for Multiphoton Imaging, Prodrug Delivery, and Chemo-Photothermal Therapy Platforms. *ACS Appl. Mater. Interfaces* **2015**, *7*, 25259-25269.

(17) Song, J.; Yang, X.; Jacobson, O.; Huang, P.; Sun, X.; Lin, L.; Yan, X.; Niu, G.; Ma, Q.; Chen, X. Ultrasmall Gold Nanorod Vesicles with Enhanced Tumor Accumulation and Fast Excretion from the Body for Cancer Therapy. *Adv. Mater*. **2015**, *27*, 4910-4917.

(18) Deng, H.; Dai, F.; Ma, G.; Zhang, X. Theranostic Gold Nanomicelles Made from Biocompatible Comb-like Polymers for Thermochemotherapy and Multifunctional Imaging with Rapid Clearance. *Adv. Mater*. **2015**, *27*, 3645–3653.

(19) Liu, X.; Chen, Y.; Li, H.; Huang, N.; Jin, Q.; Ren, K.; Ji, J. Enhanced Retention and Cellular Uptake of Nanoparticles in Tumors by Controlling Their Aggregation Behavior. *ACS Nano* **2013**, *7*, 6244–6257.

(20) Nam, J.; Wom, N.; Jin, H.; Chung, H.; Kim, S. pH-Induced Aggregation of Gold Nanoparticles for Photothermal Cancer Therapy. *J. Am. Chem. Soc.* **2009**, *131*, 13639-13654.

(21) Li, H.; Liu, X.; Huang, N.; Ren, K.; Jin, Q.; Ji, J. "Mixed-charge Self-Assembled Monolayers" as A Facile Method to Design pH-induced Aggregation of Large Gold Nanoparticles for Near-Infrared Photothermal Cancer Therapy. *ACS Appl. Mater. Interfaces* **2014**, *6*, 18930-18937.

(22) Vaupel, P.; Kallinowski, F.; Okunieff P. Blood Flow, Oxygen and Nutrient Supply, and Metabolic Microenvironment of Human Tumors: A Review. *Cancer Res.* **1989**, *49*, 6449-6465.

(23) Prabhakar, U.; Maeda, H.; Jain, R. K.; Sevick-Muraca, E. M.; Zamboni, W.; Farokhzad, O. C.; Barry, S. T.; Gabizon, A.; Grodzinski, P.; Blakey, D. C. Challenges and Key Considerations of the Enhanced Permeability and Retention Effect for Nanomedicine Drug Delivery in Oncology. *Cancer Res.* **2013**, *73*, 2412-2417.

(24) Chauhan, V.; Jain, R. K. Strategies for Advancing Cancer Nanomedicine. *Nat. Mater.* **2013**, *12*, 958-962.

(25) Sun, M.; Liu, F.; Zhu, Y.; Wang, W.; Hu, J.; Liu, J.; Dai, Z.; Wang, K.; Wei, Y.; Bai, J.; Gao, W. Salt-induced Aggregation of Gold Nanoparticles for Photoacoustic Imaging and Photothermal Therapy of Cancer. *Nanoscale* **2016**, *8*, 4452-4457.

(26) Urry, D. W. Physical Chemistry of Biological Free Energy Transduction as Demonstrated by Elastic Protein-based Polymers. *J Phys. Chem. B* **1997**, *101*, 11007-11028.

(27) Yamaoka, T.; Tamura, T.; Seto, Y.; Tada, T.; Kunugi, S.; Tirrell, D. A. Mechanism for the Phase Transition of a Genetically Engineered Elastin Model Peptide $(VPGIG)_{40}$ in Aqueous Solution. *Biomacromolecules* **2003**, *4*, 1680-1685.

(28) Liu, W.; McDaniel, J.; Li, X.; Asai, D.; Quiroz, F. G.; Schaal, J.; Park, J. S.; Zalutsky, M.; Chilkoti, A. Brachytherapy Using Injectable Seeds That Are Self-assembled from Genetically Encoded Polypeptides In Situ. *Cancer Res*. **2012**, *72*, 5956-5965.

(29) Amiram, M.; Luginbuhl, K. M.; Li, X.; Feinglos, M. N.; Chilkoti, A. Injectable Protease-operated Depots of Glucagon-like Peptide-1 Provide Extended and Tunable Glucose Control. *Proc. Natl. Acad. Sci. U.S. A.* **2013**, *110*, 2792-2797.

(30) Urry, D. W.; Parker, T. M.; Reid, M. C.; Gowda, D. C. Biocompatibility of the Bioelastic Materials, Poly (GVGVP) and Its γ-Irradiation Cross-linked Matrix: Summary of Generic Biological Test Results. *J. Bioact. Compat. Polym.* **1991**, *6*, 263-282.

(31) Ong, S. R.; Trabbic-Carlson, K. A.; Nettles, D. L.; Lim, D. W.; Chilkoti, A.; Setton, L. A. Epitope Tagging for Tacking Elastin-like Polypeptides. *Biomaterials* **2006**, *27*, 1930-1935.

(32) Urry, D. W. Elastic Molecular Machines in Metabolism and Soft-tissue Restoration. *Trends Biotechnol*. **1999**, *17*, 249-257.

(33) Liu, W.; Dreher, M. R.; Furgeson, D. Y.; Peixoto, K. V.; Yuan, H.; Zalutsky, M. R.; Chilkoti, A. Tumor Accumulation, Degradation and Pharmacokinetics of Elastin-like Polypeptides in Nude Mice. *J. Controlled Release* **2006**, *116*, 170–178

(34) Meyer, D. E.; Chilkoti, A. Purification of Recombinant Proteins by Fusion with Thermally-responsive Polypeptides. *Nat. Biotechnol*. **1999**, *17*, 1112-1115.

(35) Gao, W.; Liu, W.; Christensen, T.; Zalutsky, M. R.; Chilkoti, A. In Situ Growth of a PEG-like Polymer from the C Terminus of an Intein Fusion Protein Improves Pharmacokinetics and Tumor Accumulation. *Proc. Natl. Acad. Sci. U. S. A.* **2010**, *107*, 16432-16437.

(36) Gil, E. S.; Hudson, S. M. Stimuli-reponsive Polymers and Their Bioconjugates. *Prog. Polym. Sci*. **2004**, *29*, 1173-1222.

(37) Lian, X.; Jin, J.; Tian, J.; Zhao, H. Thermoresponsive Nanohydrogels Cross-linked by Gold Nanoparticles. *ACS Appl. Mater. Interfaces* **2010**, *2(8)*, 2261-2268.

(38) Lutz, J. F. Polymerization of Oligo (Ethylene Glycol)(Meth) Acrylates: Toward New Generations of Smart Biocompatible Materials. *J. Polym. Sci., Part A: Polym. Chem*. **2008**, *46*, 3459-3470.

(39) McDaniel, J. R.; MacKay, J. A.; Quiroz, F. G.; Chilkoti, A. Recursive Directional Ligation by Plasmid Reconstruction Allows Rapid and Seamless Cloning of Oligomeric Genes. *Biomacromolecules* **2010**, *11*, 944-952.

(40) MacKay, J. A.; Chen, M.; McDaniel, J. R.; Liu, W.; Simnick, A. J.; Chilkoti, A. Self-assembling Chimeric Polypeptide-doxorubicin Conjugate Nanoparticles That Abolish Tumours after a Single Injection. *Nat. Mater*. **2009**, *8*, 993-999.

(41) Lin, M.; Guo, C.; Li, J.; Zhou, D.; Liu, K.; Zhang, X.; Xu, T.; Zhang, H.; Wang, L.; Yang, B. Polypyrrole-Coated Chainlike Gold Nanoparticle Architectures with the 808 nm Photothermal Transduction Efficiency up to 70%. *ACS Appl. Mater. Interfaces* **2014**, *6*, 5860-5868.

(42) Ghosh, S. K.; Pal, T. Interparticle Coupling Effect on the Surface Plasmon Resonance of Gold Nanoparticles: from Theory to Applications. *Chem. Rev*. **2007**, *107*, 4797-4862.

(43) American National Standards Institute. In *American National Standard for the Safe Use of Lasers*; Laser Institute: Orlando, FL, **1993**; Vol. ANSI Z136 1-1993.

(44) Albanese, A.; Tang, P. S.; Chan, W. C. W. The Effect of Nanoparticle Size, Shape, and Surface Chemistry on Biological Systems. *Annu. Rev. Biomed. Eng.* **2012**, *14*, 1–16.

(45) Jong, W. H. De; Hagens, W. I.; Krystek, P.; Burger, M. C.; Sips, A. J. A. M.; Geertsma, R. E. Particle Size-dependent Organ Distribution of Gold Nanoparticles After Intravenous Administration. *Biomaterials* **2008**, *29*, 1912-1919.

ToC graphic: